

Combustion-formed nanoparticles

Andrea D'Anna *

Dipartimento di Ingegneria Chimica, Università "Federico II" di Napoli, Piazzale V. Tecchio, 80, 80125 Napoli, Italy

Abstract

The processes by which carbonaceous nanoparticles are produced from combustion of liquid and gaseous fuels are reviewed. The focus of the paper is on the formation and properties of nanoparticles in laboratory laminar, premixed and diffusion flames and on the most popular methods of sampling and detection of these particles. Particle chemical nature is analyzed from data obtained by several measurement techniques. Measurements characterizing nanoparticles in the exhausts of practical combustion systems such as engines and commercial burners are also reported. Two classes of carbonaceous material are mainly formed in combustion: nanoparticles with sizes in the range 1–5 nm, and soot particles, with sizes from 10 to 100 nm. Nanoparticles show unique chemical composition and morphology; they maintain molecular characteristics in terms of chemical reactivity, but at the same time exhibit transport and surface related phenomena typical of particles. The emission of these particles contributes to atmospheric pollution and constitutes a serious health concern. A simplified modeling analysis is used to show how the growth of aromatics and the chemical nature of the particles depend on temperature and radical concentration distributions encountered in flames.

© 2009 The Combustion Institute. Published by Elsevier Inc. All rights reserved.

Keywords: Nanoparticles; Flames; Diagnostic; Modeling

1. Introduction

Combustion of fossil fuels and biomass generates particulate matter ranging from micrometer-sized aggregates down to fine and ultrafine particles in the nanometer-sized range. The largest particles mainly derive from the physical transformation of the inorganic fraction of the fuel in the form of ash, or result from the agglomeration of fine and ultrafine particles nucleating from the gas-phase in the high temperature environment. These particles can be success-

fully removed from combustion exhausts in suitable gas-cleaning devices.

Particles formed at high-temperature gas-to-particle transitions are of nanometric size, difficult to intercept in the gas-cleaning devices and thus contributing to air pollution. They are often referred to as nanoparticles or ultrafine particles. The emission of these particles in the atmosphere constitutes a serious concern for our health and for their contribution to photochemical smog. The smallest particles play a particularly important role in health since they dominate size distributions in terms of number concentration and are they able to penetrate deeper than larger particles into the respiratory system [1–3]. They could also affect the radiation balance of the atmosphere by serving as condensation nuclei for the formation of clouds and of contrails in the upper atmosphere [4].

* Fax: +39 081 593 6936.

E-mail address: andrea.danna@unina.it

Emission of nanoparticles in the atmosphere is of central interest in the field of atmospheric chemistry provoking debate on the relative role of primary particles, directly emitted from combustion systems in the form of volatile organic carbon and nanoparticles, and secondary particles formed from combustion products through atmospheric reactions [5–8]. The mechanisms of formation and the physical and chemical characteristics of primary particles are not completely clear. We have the specific task of providing a detailed characterization of primary particles from vehicles and stationary combustion sources for studies of atmospheric chemistry and toxicology.

Combustion generated nanoparticles have a unique chemical composition and morphology since they maintain molecular characteristics in terms of chemical reactivity, but at the same time exhibit transport and surface related phenomena typical of particles. Many new diagnostic tools, which allow analysis on an almost atomic level have been developed, or borrowed from molecule-based natural sciences. Their use improves our knowledge about the physical and chemical properties of combustion-formed nanoparticles and also about the kinetics of particle formation in combustion environments.

Details about the formation of particles in combustion, particularly soot particles, have been reported in many research papers, comprehensive reviews [9–12] and in published round-table discussions on soot held in the last 30 years [13–17]. The present topical review focuses on the processes by which carbonaceous nanoparticles with a diameter of 1–100 nm are produced from combustion of liquid and gaseous fuels. The paper mainly addresses formation and properties of nanoparticles in laminar, premixed and diffusion flames. Section 2 describes methods of sampling and detection for particles in the size range of interest. Also, particle chemical nature is analyzed based on information gained from several measurement techniques. Sections 3 and 4 deal with the formation of nanoparticles in premixed and non-premixed laboratory flames. Measurements characterizing nanoparticles in the exhausts of practical combustion systems such as engines and commercial burners are reported in Section 5. Finally in Section 6 a model of nanoparticle nucleation from the gas phase and particle growth in different combustion environments is discussed. The model is used to show how the growth of aromatics and the chemical nature of the particles depend on temperature and radical concentrations in the flames.

2. Diagnostics for particles

Combustion-formed particles range in size from near molecular dimensions up to some hun-

dreds of nanometers and require an array of techniques for detailed chemical and physical characterization. The smallest particles, behaving like molecules, show spectroscopic properties such as absorption and fluorescence, which allow either identification of their chemical functionalities and/or their quantification both in-situ and in the sampled material. The very low molecular mass associated with these particles makes the size measurements quite difficult. Interaction of light with particles results in static or dynamic light scattering. Static scattering from very small particles is of the same order of magnitude as scattering from the gas-phase products in which the particles are suspended making this technique unsuitable. Diagnostics based on the detection of dynamic emissions, both scattering and fluorescence, improves the size measurement capability in the nanometer-sized range. Larger particles are more suitable for laser induced incandescence and laser light scattering measurements. These two measurements together allow the direct evaluation of particle concentration and size distributions in combustion systems, although enormous difficulties can arise in experimental implementation of these diagnostics and the data interpretation.

Although in-situ measurements of nanoparticles are important for the determination of particle formation kinetics, additional structural and morphologic information is also of great interest to characterize combustion-formed particles and assess their role on the environment and on human health. This information is better retrieved from particle samples collected in the combustion systems and analyzed by off-line techniques. However, careful sampling is required to avoid artifacts formed from chemical and physical interactions during the collection and handling procedure.

The combination of ex-situ and in-situ measurements can lead to a thorough characterization of particles in the whole size range. A description of the methods currently used for combustion-formed nanoparticles is reported here. No claim of completeness is made and there are some further diagnostic techniques for particles not discussed here which would require as much attention again.

In-situ diagnostics exploit the interaction of light with particles in the combustion environment. Extensive extinction measurements in the visible range have been made using pulsed or continuous laser sources [18] to obtain the volume fraction of soot, defined as visible absorbing particles of any size. In the Rayleigh approximation, knowing the optical properties of the particles through the complex refractive index m_i , the volume fraction of visible absorbing particles, soot, (f_V) is determined from extinction measurements (K_{ext}) at a fixed wavelength (λ) in the visible by the relations:

$$K_{\text{ext}} = -\frac{\pi^2}{\lambda} \sum \text{Im} \left(\frac{m_i^2 - 1}{m_i^2 + 2} \right) N_i d_i^3 \quad (1)$$

$$f_V = \sum N_i \frac{\pi d_i^3}{6} \quad (2)$$

Particles which do not absorb light in the visible are not detected by this procedure. In recent years D'Alessio et al. [19] developed a broad-band absorption technique in order to also detect species which are transparent to visible radiation, but are strongly absorbing in the ultraviolet. These may be incipient particles which still retain a molecular structure. Light sources with a continuous spectrum from 190 nm up to 800 nm allow measurements in the whole spectral range [19–23].

Absorption spectra in the UV can be attributed to a variety of compounds. Many of them are in the gas-phase: CO₂ and H₂O strongly absorb light in the UV at high temperatures [24,25]. Aromatic compounds in gas-phase or as condensed matter also absorb UV light [26–28]. The contribution of the gas-phase aromatic compounds as well as CO₂ and H₂O can be estimated by measuring or modeling their concentration and their specific absorbance at flame temperatures. Excess absorption is then attributed to particles. By using Eq. (1) in the whole wavelength range it is possible to estimate the volume fractions of classes of particles once their wavelength-dependent optical properties are known. This procedure has been successfully used to define two classes of absorbing particles: nanoparticles of organic carbon which absorb light in the UV up to about 350 nm and soot particles whose absorption extends down to the visible [19–23].

By combining extinction measurements with scattering measurements it is possible to determine the mean size of the particles. In the Rayleigh approximation the scattering signal is proportional to the product of particle volume fraction and the cube of diameter through the relation:

$$Q_{\text{vv}} = \frac{\pi^4}{4\lambda^4} \sum \left| \frac{m_i^2 - 1}{m_i^2 + 2} \right|^2 N_i d_i^6 \quad (3)$$

From Eqs. (3) and (1), the ratio of the sixth-to-third moment of the size distribution function is obtained:

$$d63 = \left(\frac{(\sum N_i d_i^6)}{(\sum N_i d_i^3)} \right)^{1/3} \quad (4)$$

When both nanoparticles and soot are simultaneously present measurements at different wavelengths are necessary to get the average size and volume fractions for both particle classes. Also the scattering from gas-phase compounds must be subtracted from the measured values [20].

In-situ optical methods are useful tools for particle detection without intrusive sampling, but

they are strongly affected by interference from gaseous products and by the choice of the wavelength-dependent particle refractive index which depends on the chemical nature of the particle itself.

Light scattering is related to the real part of the refractive index, whereas extinction is strongly correlated with its imaginary part. A further laser based diagnostic for particles, based on the absorptive imaginary part of the refractive index, is Laser Induced Incandescence (LII) [29–34]. Particles are heated up by a short and intense laser pulse and the particle thermal radiation is related to the volume fraction of the particles; the time behavior of the signal during the cooling-down to the temperature of the surrounding gases is correlated with particle sizes. Quantitative calibration is typically obtained by reference to an extinction measurement. This technique has been successfully used for the characterization of primary soot particles in laboratory flames and in more complex industrial devices [32,33,35].

Light sources in the UV can also induce electronic transitions and subsequent emission of fluorescence in specific classes of molecules such as polycyclic aromatic hydrocarbons (PAH) and oxygen-containing compounds [36–43]. For nanoparticles, exhibiting molecular characteristics, Laser Induced Fluorescence (LIF) may also be a useful detection tool [44–46]. Non-premixed flames and turbulent combustion conditions need spatial resolution. Here LIF and LII measurements employing pulsed laser sources are superior to absorption measurements which need tomographical inversion [45,47].

LIF spectra of nanoparticles are similar to those exhibited by molecules such as polycyclic aromatic hydrocarbons (PAH), so that particle discrimination is difficult. Therefore, it is necessary to exploit some properties of fluorescence, which depend unequivocally on particle size, so that both chemical characteristics and size can be determined. This goal is achieved by performing time-resolved fluorescence polarization anisotropy (TRFPA) measurements [48–50]. The technique allows the retrieval of size and spectral characteristics of the particles. The probe volume is irradiated with ultrafast, linearly polarized, laser radiation pulses and the time evolution of the two polarization components (parallel and orthogonal to the exciting field) of the broadband fluorescence emission is analysed. Fluorescence emission has the same polarization as the laser beam, but the degree of polarization is reduced within a time-scale of hundred of picoseconds due to the rotational motion of the fluorescing species. The characteristic decay time of the depolarization is dependent on the volume and the shape of the fluorescing particles. Thus, by measuring fluorescence depolarization, it is possible to determine the ensemble-averaged size and

shape of all fluorescing particles. The technique is also able to determine dimensions of various particles in a polydispersed sample, provided that particles with different sizes also have different spectral properties. It has to be underlined that this powerful tool is limited by the requirement that particles/molecules have to exhibit fluorescence and it requires the use of sophisticated ultrafast laser sources.

Another diagnostic method is dynamic light scattering (DLS), which has been used to measure soot particle size in flames [51,52]. The scattered light spectrum is broadened by the particle Brownian motion which is particle size dependent. DLS is independent of the refractive index of the particles and, within certain limits, can also furnish additional information on particle size distribution. Depolarized DLS may also provide global shape information. However, fluorescence emission can interfere with the scattered signal.

A complete overview of the current state-of-the-art of in-situ laser-based optical diagnostics for particle characterization is reported in ref. [53].

Real-time, partially interfering techniques can also be used for the characterization of combustion-formed particles.

Differential Mobility Analysis (DMA) is becoming a widely accepted tool for the determination of the size distribution of the particles extracted from the flame without any manipulation of the sample [54–59]. DMA measurements require a high dilution sampling system to reduce the sample temperature and concentration and to avoid further reactions and particle coagulation in the sampling line. Particles are charged and separated in an electrostatic classifier based on their electrical mobility. A mobility, or size distribution is determined by counting the charged particles which exit the classifier, varying the applied voltage. When state of the art instrumentation is used, a size distribution from 1 to 100 nm can be measured [59,60]. The accuracy of the measurement relies on the correct evaluation of the dilution ratio required to suppress particle coagulation in the sampling line, charging efficiency and particle losses through the sampling lines/instrument. This is particularly problematic for particles down to 10 nm. Diffusion losses and the interpretation of particle mobility in terms of size are critical points [60]. Also DMA is not able to qualify the result as a function of particle chemical nature.

Information on the molecular mass and structure of the particles can be retrieved by molecular-beam, time-of-flight (MB-TOF) sampling. This has the advantage of an on-line method with only weak disturbance to the reacting flow. A sample is supersonically expanded into a vacuum chamber; the flow conditions are such that the gas temperature decreases rapidly freezing chemical and physical processes almost completely [61]. MB-TOF coupled with a mass spectrometer (MB-TOF-

MS) is a useful tool for studying nanoparticle formation in combustion. Naturally ionized particles/molecules are immediately detected by a TOF-MS [62–64], whereas neutral particles present in the molecular beam need to be ionized first by a multiphoton ionization process and then they can be analyzed by a TOF-MS [65–68]. Different photo-ionization thresholds can be used to distinguish between particles having the same molecular mass but different chemical nature. This is achieved by adjusting the wavelength and the energy of the laser not only as a function of the mass range investigated, but also for the types of bonding in the particle [69]. In order to obtain quantitative results this method needs to be calibrated for a very large number of compounds.

Particles collected in the combustion environment can also be analysed for their chemical and physical characterization by off-line measurements. Sampling procedure is the crucial point: the procedure should not falsify or change the particle properties in order that the sampled material be representative of the particles in the combustion environment. Although many precautions are adopted the collection procedure inevitably modifies the samples and information obtained from off-line characterization of the sampled material has to account for possible sample modifications.

A way to withdrawn particles from combustion environments is by using suction probes. Combustion products are isokinetically sampled by means of water-cooled probes; total particle collected on the probe wall, on filters and in ice-cooled traps placed in the sampling line is extracted by solvents in order to separate the soluble species from soot. Soot samples are dried, weighed and suspended by ultrasonic agitation in suitable solvents for further analysis [70–72]. The soluble species are usually analyzed by high pressure liquid chromatography and mass spectrometry for the quantification of gas-phase PAH [71,72]. UV-visible absorption and fluorescence measurements are then used for the chemical characterization of the other absorbing and fluorescing species [73–75].

Size Exclusion Chromatography (SEC) analysis is used for the evaluation of molecular mass distribution of the sampled material [76–80]. SEC is performed by using a High Pressure Liquid Chromatograph equipped with a diode array detector for absorbance measurements. A calibration curve is used to determine the molecular mass of the particles.

Fourier-Transformed Infrared (FTIR) analysis and Surface-Enhanced Raman Scattering (SERS) have been employed to characterize nanoparticles produced in combustion by batch or in-situ [72,81–83]. The measured spectral features supply insight on the chemical properties of the combustion products through the identification of CC,

CH and CO bonding. Coupled elemental analysis also gives information on the amount of C and H atoms in the samples [74,84].

Analysis of particle mobility can also be performed in batch on material sampled from the flame and dispersed in solvents. In this case an electrospray coupled with a differential mobility analyzer can be used to determine size of suspended nanoparticles [85,86]. Measurements of the size distribution functions of the particles suspended in a solvent can be also performed by taking advantage of DLS [87] and TRFPA [49]. In this way size distributions can be obtained by matching results obtained with different techniques and based on independent parameters.

Another common way of collecting particles is thermophoretic sampling. A cold surface placed in line with flow streamlines produces a strong temperature gradient making particles move towards the surface by thermophoretic forces [88,89]. Thermophoretic drift velocity is independent of particle size, but not the capability of a particle to stick to the surface [90]. Cool substrates can be inserted into flames with a sampling time of few milliseconds in order to reduce flame perturbation. The collected samples can undergo spectroscopic characterization and microscopy analysis and chemical composition can be obtained by sensitive Laser Microprobe Mass Spectrometry (LMMS) [91], or by spectral absorption and fluorescence measurements [74].

Size distribution functions of the particles deposited on substrates can be obtained by High-Resolution Transmission Electron Microscopy (HR-TEM) [84,92,93] and Atomic Force Microscopy (AFM) [90,94]. AFM furnishes a 3D topological map of particles deposited on atomically flat substrates, with angstrom resolution in height and nanometer resolution in the plane parallel to the surface [94]. This is a great advance relative to other microscopy techniques such as TEM which only gives a 2D characterization of the particles. AFM operating in tapping mode collects a three dimensional map of the sample by precisely monitoring the position of a cantilever beam with a laser as it vibrates along the surface of the sample without having to further coat the sample. The vibrating tip of the cantilever beam is ideally ending in one atom. Determination of the interactions between the cantilever and the samples can also reveal information about the viscoelastic properties of the collected material [95].

3. Nanoparticles in laminar premixed flames

Laminar premixed flames are the preferred laboratory systems to study the kinetics of particle formation. Usually they operate at steady state, and the combustion conditions can be easily var-

ied. Simple fluid-dynamics allows processes to be followed along the flame axis to obtain kinetics data. Modeling can be performed using detailed kinetic schemes containing hundreds of species and thousands of reactions.

Many experimental studies in premixed flames have been restricted to the analysis of soot formation because the diagnostics were not sensitive enough to detect particles smaller than soot.

Fuel-rich premixed hydrocarbon flames exhibit a typical luminous structure: a blue region close to the burner due to the large formation of OH radicals in the flame front followed by an almost transparent region and downstream by a zone with intense yellow-orange luminosity. This zone becomes more evident as the C/O ratio of the fuel-air mixture is increased. The transparent region is observed in flames of aliphatic hydrocarbons, but vanishes for an aromatic fuel because the yellow-orange zone overlaps with the blue zone.

The flame luminosity structure is well described by the elastic laser light scattering along the flame axis. Figure 1 reports the scattered light signal intensity along the flame axis of a C/O = 0.77 ethylene/air flame with a cold-gas flow velocity of 10 cm/s which is here taken as a test case [20,22]. A strong scattering signal is detected at the exit of the burner; it decreases moving away from the burner exit up to a minimum value followed by a plateau region and a strong scattering region downstream. The decrease of the scattering signal is due to the increase of the flame temperature in the region of the intense blue luminosity, the plateau region corresponds to the transparent region and the strong increase of the scattering signal corresponds with the yellow-orange luminosity.

Scattering signal can be attributed to gas and condensed phases on the basis of the extinction

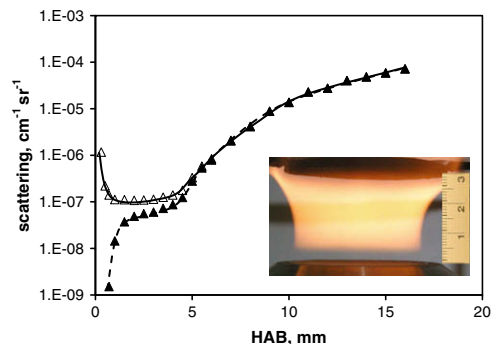


Fig. 1. Scattered light signal intensity at 266 nm (Δ) measured along the flame axis of a slightly-sooting, C/O = 0.77, ethylene/air flame with a cold gas flow velocity of 10 cm/s. \blacktriangle represents the scattering in excess to gaseous species.

spectra. The spectrum measured in the blue region of the flame shows a UV signal which decays at increasing wavelength and vanishes at about 300 nm. Moving downstream from the flame location, the UV signal increases and some absorption in the visible starts to be detected. The visible absorption becomes significant at higher flame heights in the yellow-orange region. Figure 2 shows typical extinction spectra measured in the C/O = 0.77 ethylene flame at two locations, namely 4 mm, in the transparent region downstream of the flame zone (Fig. 2 – upper part) and 8 mm, in the yellow-orange zone (Fig. 2 – lower part). The UV absorption in the range 200–250 nm can be attributed to H₂O and CO₂ molecules which have been found to exhibit strong absorption at high temperature [24,25]. Figure 2 reports as dashed lines the contribution of CO₂ and water molecules to the absorption spectra estimated from gas concentrations predicted by kinetic modeling and estimated absorption cross sections at flame temperatures. The absorption in the visible range reported in the lower part of Fig. 2 is due to soot particles. In the UV the contribution of soot particles to absorption can be estimated from the typical absorption spectrum of soot measured on a quartz

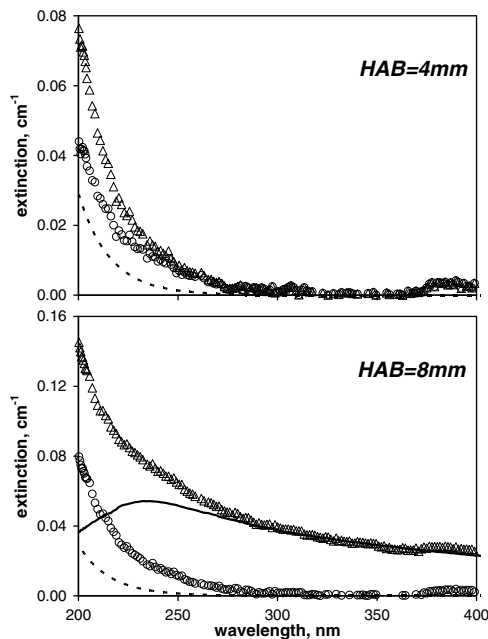


Fig. 2. Extinction spectra measured at 4 mm (upper) and 8 mm (lower) from the burner outlet in a slightly-sooting, C/O = 0.77, ethylene/air flame with a cold gas flow velocity of 10 cm/s. Δ represents the measured data; dashed lines are the contribution of CO₂ and H₂O to the extinction spectrum; continuous line is the typical absorption spectrum of soot; \circ represents the extinction subtracted by the contribution of soot, CO₂ and H₂O.

disk reported as a thin line in the Figure. By subtracting the contribution of gaseous products and soot absorption from the spectra of Fig. 2 there is still extra absorption in the UV which has to be attributed to other UV-absorbing, visible-transparent molecules/particles. It is interesting to note that the spectral behavior of the excess absorption in the UV remains quite unchanged in the two flame locations reported in Fig. 2; it shows strong absorption in the UV which decays at increasing wavelength and vanishes at about 300 nm.

Taking advantage of the clearly distinct spectral behavior between soot and visible-transparent species it is possible to follow their evolution along the flame axis. Volume fractions of the two classes of species, mean diameters (d_{63}) and number concentrations have been calculated from excess-scattering to gaseous compounds (Fig. 1) and extinction measurements from Eqs. (1)–(4), and known optical properties. The refractive indices used for soot are the well known values of Dalzell and Sarofim [96] and Chang and Charalampopoulos [97]: $m_{\text{soot}}(\lambda = 532 \text{ nm}) = 1.57 - i0.56$, $m_{\text{soot}}(\lambda = 266 \text{ nm}) = 1.4 - i0.75$, whereas the value used for nanoparticles is that evaluated by Cecere et al. [87]: $m_{\text{vis-transparent}}(\lambda = 266 \text{ nm}) = 1.4 - i0.08$.

Just downstream of the main reaction zone of the flame, the volume fraction of visible-transparent species increases and a large number concentration of particles of the order of 10^{13} cm^{-3} is observed. Particle size does not exceed 3 nm, as demonstrated by the low scattering measured in excess to gaseous compounds reported in Fig. 1, and the spectral behaviour is limited to UV wavelengths (Fig. 2 – upper part). Beyond the maximum value, the volume fraction of visible-transparent species decreases in correspondence with the formation of visible-absorbing, soot particles. These have a much lower number concentration of the order of 10^{11} cm^{-3} but larger sizes ranging from 5 to 25 nm. Optical measurements do not allow determination of size and number concentration of the two classes of particles simultaneously because scattering is biased to the larger particles and the contribution to the scattering of the smaller particles become negligible. The number concentration and mean size reported in the Figure for the smaller particles have been calculated in the transparent region of the flame where larger particles are absent. The size of the visible-transparent particles was considered unchanged along the flame axis. Figure 3 shows the estimated number concentration and mean size of smaller particles in the yellow-orange region of the flame as dashed lines.

The volume fraction of total particles is also reported (sum of soot and visible-transparent particle volume fractions). Beyond the maximum value at the end of the transparent region it remains quite constant in the yellow-orange

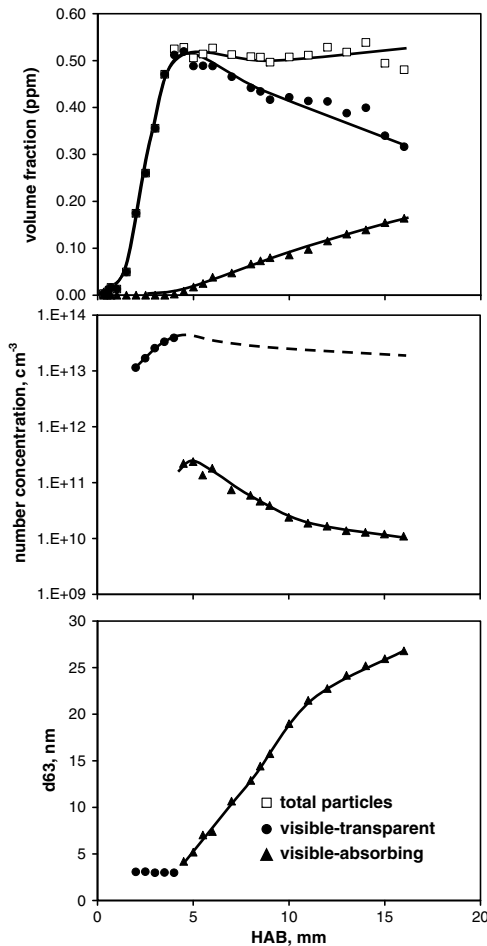


Fig. 3. Volume fractions (upper), number concentration (intermediate) and mean sizes (lower) of visible transparent (●) and visible-absorbing (▲) species along the flame axis of a slightly-sooting, $C/O = 0.77$, ethylene/air flame with a cold gas flow velocity of 10 cm/s. □ represents the total volume fraction.

region indicating that soot particles derive directly from the chemical transformation and coagulation of visible-transparent particles at least in slightly-sooting flames.

Laser induced fluorescence (LIF) spectra measured at the same locations of the absorption measurements can help qualify the chemical nature of the formed particles. Figure 4 reports the LIF spectra measured at 4 mm and 8 mm in the $C/O = 0.77$ ethylene flame with an excitation wavelength of 266 nm. The LIF spectrum measured after the flame front in the transparent region of the flame shows the scattering signal at 266 nm and residuals of the second harmonic of the laser at 532 nm, a broad signal in the region between 290 and 400 nm with a maximum at about 320. The spectrum measured in the yellow-

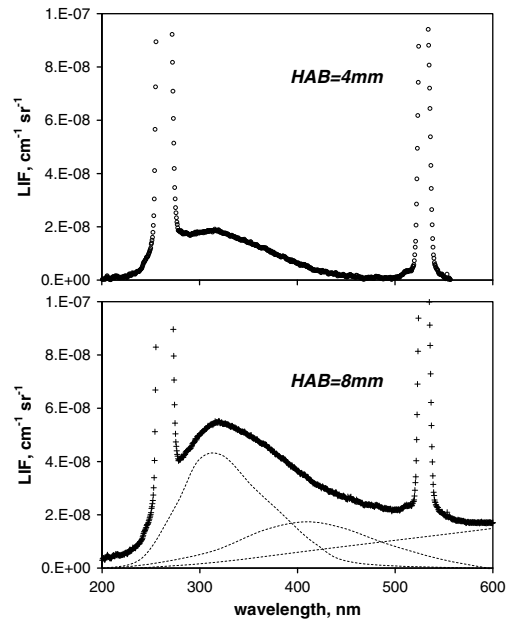


Fig. 4. Fluorescence spectra induced by laser radiation at 266 nm measured at 4 mm (upper) and 8 mm (lower) from the burner outlet in the $C/O = 0.77$ ethylene/air flame. Dashed lines represent the contributions of UV and visible fluorescence and of incandescence of particles.

low-orange region shows a fluorescence signal which extends down to 500 nm and a continuum which extends above the 600 nm. The spectral behavior between 290 and 600 nm can be de-convoluted into two broad fluorescence bands: the first has a shape similar to that measured at 4 mm and reported in the upper part of Fig. 4 whereas the second is broadband with a maximum at 420 nm. Both bands are typical of fluorescence from aromatic compounds whereas the continuum background which extends into the visible can be attributable to incandescence of soot particles.

Optical data unambiguously show the presence of two classes of particles: precursor nanoparticles with mean sizes between 2 and 4 nm, transparent to the visible radiation and fluorescing in the UV, and visible absorbing particles, referred to as soot, with mean sizes between 5 and 20 nm. Visible fluorescence detected in the yellow-orange region of the flame may be attributed to young soot particles or to precursor nanoparticles in their transformation to soot.

The first in-situ evidence of precursor nanoparticles in premixed flames came from the mass spectrometric studies of Homann and Wagner [65] in the early sixties. They had evidence of “reactive polycyclic hydrocarbons probably with side-chains, containing more hydrogen than aromatic

(mass range ≈ 150 to >550)". Their presence has been confirmed by MB-TOF-MS studies of ions performed by Homann and co-workers [62–64,66] and lately by the photo-ionization TOF-MS analysis of Grotheer [67] on neutral species. Homann hypothesized that the high-mass species with molecular masses ranging from 600 to 2500u were PAHs containing 5-membered rings held together mainly by van der Waals-forces or occasionally by a C–C bond or chain. The spectroscopic behaviors of precursor nanoparticles detected in flames support and confirm the Homann hypothesis. Indeed spectral behaviour limited to the UV wavelengths suggests that nanoparticles are constituted by aromatic species with a maximum of 2–3 ring chromophores connected by sp³ bonding [19,23].

Off-line measurements have supported the presence of nanoparticles in flame. In a pioneering work, Zhao et al. [54] measured, with a differential mobility analyser, nanoparticles with sizes down to 3 nm (the limit of the measuring device) in the soot preinception region of a nearly-sooting ethylene flame. Particle size distribution evolved towards a bimodal shape when soot particles were formed. Lately, measurements have been performed with a state of the art measuring device and sampling line able to measure particles with sizes as low as 1 nm [59]. Figure 5 reports the particle size distribution functions detected just downstream of the flame front of the C/O = 0.77 ethylene flame and at higher heights where the visible absorption is also detected. A rather mono-disperse peak with a modal mobility diameter of about 2 nm and a standard deviation of about 0.8 is detected just downstream of the flame front whereas a second mode with diameters larger than 10 nm is observed late in the post-oxidation zone [59]. The smallest mode is measured in conditions where the extinction and fluores-

cence spectra are limited to the far UV with very low values of scattering in excess to gaseous compounds. When a significant extinction in the visible wavelength range is detected and the scattering increases by orders of magnitude, the size distribution function includes a second mode with mobility diameters larger than 10 nm, in addition to the smaller peak associated with nanoparticles.

It is worth noting that when soot particles are detected, the first mode of the particle size distribution also includes nanoparticles with sizes around 5–8 nm indicating a continuous coagulation of nanoparticle in the process of soot formation.

It is quite difficult to accurately measure the particle size distribution in flames. Indeed, a high dilution of the sample is required to avoid particle coagulation of the first mode in the sampling line. This high dilution ratio causes the concentration of the second mode of particles to be around the detection limit of the instrument. The total particle number concentration even in moderately sooting flames saturates the particle charger, and the amount of ion-pairs in the charger is not enough to fully charge the aerosol to the so-called steady state charge distribution rendering the measurement quantitatively inaccurate. Another large source of error is the blockage of the probe orifice in soot-forming flames. The orifice closes much faster (within some seconds) than the scan time of the measurement (some minutes) causing a decrease of the detection signal. Interestingly, in flames that produce only nanoparticles, the measured signals does not change in the time associated with the measurements even when the amount of sampled material is high enough to block the sampling hole entirely in few seconds. This observation may indicate that small particles do not stick readily to the probe surface probably because of thermal rebound from the metal.

Thermal rebound of the smaller particles is probably also the reason for the low coagulation rate of nanoparticles measured in flames. Indeed in flames with C/O ratios below the detection of visible absorption, the particle size distribution does not change in time as fast as if all collisions resulted in particle coagulation. DMA measurements as a function of height above the burner find that the coagulation rate is significantly lower than the collision rate for nanoparticles at flame temperatures [98], in agreement with optical measurements. The latter also show a plateau region in scattering due to the formation of nanoparticles which are unable to undergo coagulation [20,22,90].

This interesting behavior of nanoparticles may explain why they escape exhaust systems without significant growth to larger sizes at high temperature. The measured coagulation rate of nanoparticles depends on particle size and is currently

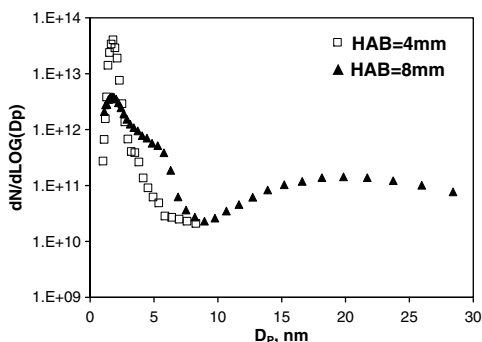


Fig. 5. Particle size distribution measured with a DMA at 4 mm (\square) and 8 mm (\blacktriangle) from the burner outlet in the C/O = 0.77 ethylene/air flame. Data are corrected by the sampling dilution and particle loss in the sampling line and in the instrument.

explained by a simple balance between van der Waals-interaction energy and the thermal kinetic energy of the particles [90]. A better understanding of the coagulation rate of nanoparticles would be useful for pollution reduction strategies, or for industrial processes designed to produce nanoparticles of controllable size.

The lower coagulation rate can be also related to the chemical nature of the particles. Indeed the presence of functional groups containing oxygen within the chemical structure of nanoparticles can change the sticking capability of the particles and hence their coagulation efficiency. If oxygen containing functionalities are present in combustion-generated nanoparticles, it is also possible to explain why nanoparticles with sizes below 3 nm remain dispersed in water samples in contrast to larger particles and more graphitic soot particles [85,86]. Functional groups containing oxygen have been observed in samples collected from flames using either Fourier Transform Infrared (FTIR) spectroscopy [72,81] or Surface-Enhanced Raman Spectroscopy (SERS) [83]. The presence of oxygen in nanoparticles is of great importance. Oxygen may also play a role in how these particles affect biological systems.

Atomic Force Microscopy (AFM) measurements of the material sampled by thermophoresis have confirmed the presence of small particles in the pre-inception region of the $C/O = 0.77$ ethylene-air flame. Figure 6 reports the particle size distribution in terms of spherical equivalent diameters, measured at 4 mm and 8 mm. The figure reports the size distribution counted by AFM corrected for the size-dependent sticking efficiency on mica surface [90].

An interesting aspect of AFM measurements is that they give the three dimensional structure of particles deposited on the substrate. All single particles measured by AFM in non-sooting and sooting flames have shown a non-spherical shape on the mica substrate. The shape in the x - y plane

is almost always circular, and the aspect ratio (maximum height/base diameter) is always less than unity. This result might suggest that the measured particles have elongated structures or they are probably spherical and they spread out on the mica substrate upon impact or over time. The degree to which the particles spread over the surface may be related to their viscoelastic properties. Figure 7 plots the aspect ratio measured for all particles sampled in the sooting flame ($C/O = 0.77$) vs. their spherical equivalent diameter. Early in the flame, where optical measurements find only 2–3 nm particles, the AFM measurements show particles with very low aspect ratios (about 0.05). Higher in the flame where a wider bimodal distribution of sizes is measured, the aspect ratio of particles larger than about 10 nm increases toward the spherical limit (aspect ratio = 1) with increasing particle sizes. AFM measurements over a wide range of operating conditions (varying C/O , flame residence times, temperatures, and hydrocarbon fuel burned) find a relationship of aspect ratio and equivalent diameter that is similar to the one reported in Fig. 7 [90,94]. The result that the smaller particles spread out more than larger particles indicates that they have a different structure; they may be more liquid and/or more polar. The elongated structures of the nanoparticles has been hypothesized in the past [19,23] by measurement of the depolarization ratio of the scattered light which shows very high values in the preinception region of the flame associated with elongated structures and shows very low values in the soot loading region of the flame associated with more spherical soot particles.

Additional information on the size distribution of the combustion-formed particles have been obtained by Size Exclusion Chromatography (SEC) coupled with on-line UV-visible detection. SEC commonly used for the determination of the molecular weights (MW) of polymeric structures, has been used to evaluate the MW distribu-

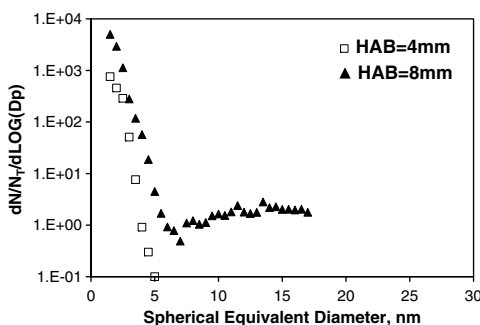


Fig. 6. Particle size distribution measured by AFM at 4 mm (□) and 8 mm (▲) from the burner outlet in the $C/O = 0.77$ ethylene/air flame. Data are corrected by the size dependent sticking efficiency.

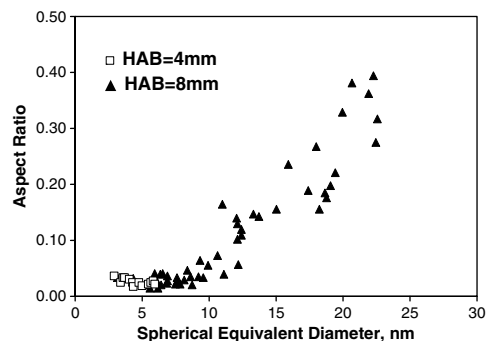


Fig. 7. Aspect ratio of the particles measured by AFM at 4 mm (□) and 8 mm (▲) from the burner outlet in the $C/O = 0.77$ ethylene/air flame.

tion of particles collected from flames [76–80]. Polystyrene standards and carbonaceous samples of well defined sizes were used for MW calibration.

Two broad peaks are observed in the species MW distribution measured in the transparent region of the flame: the first one is in the range of molecular mass between 500 and 2000 u close to the peaks of PAHs and the second one in the molecular mass region of 10^4 – 10^5 u. Considering a density of 1.2 g/cm^3 typical of PAHs, the two broad peaks correspond to particles with an equivalent spherical diameter of 1–2 and 3–7 nm, respectively. Moving downstream of the flame in the soot formation region two other peaks become prevalent. One peaks between 10^6 and 10^7 u and the other at 10^8 – 10^{10} u equivalent to spherical particles having sizes of 10–20 nm and 50–200 nm, respectively, if a density of 1.8 g/cm^3 , typical of soot, is used for these particles.

The presence of nanoparticles in flames has also been confirmed by TRFPA measurements [48,49]. This technique is only able to detect fluorescing particles since it excites fluorescence in the UV with a femtosecond laser source. It determines the rotational diffusion coefficient of species present from the measured polarization decay. Measurements on samples from the $C/O = 0.77$ flame have shown both a short and a longer decay time. They indicate the presence of particles with a mean size of 2–3 nm, exhibiting an UV peaked fluorescence, in addition to larger particles with a mean diameter of 4–8 nm, which exhibit a fluorescence shifted more to the visible. Nanoparticles with sizes of 2–3 nm are detected in the transparent region of the flame, whereas the 4–8 nm particles are detected at the beginning of the appearance of yellow-orange luminosity.

In summary, in-situ optical measurements, probe sampling and characterization in an atmospheric pressure laminar premixed flame of ethylene show that two classes of carbonaceous material are mainly formed in rich flames: nanoparticle of organic carbon and soot particles. The spectral forms of the extinction and fluorescence give an indication of the chemical nature of the particles and show that the smaller particles can be thought as polymer-like structures containing sub-structures with aliphatic and aromatic (limited to 2–3 rings) bonds and possibly oxygen. The process of soot formation seems to be the coagulation of the 2–3 nm particles, which at the same time lose H and gain a higher condensed ring number aromatic or graphitic structure.

Nanoparticles have been detected in premixed flames with C/O ratios significantly lower than the onset of soot. Figure 8 plots the total particle volume fraction determined by extinction in the UV and visible, AFM, and on-line DMA measurements at 10 mm in ethylene/air flames with different C/O ratios.

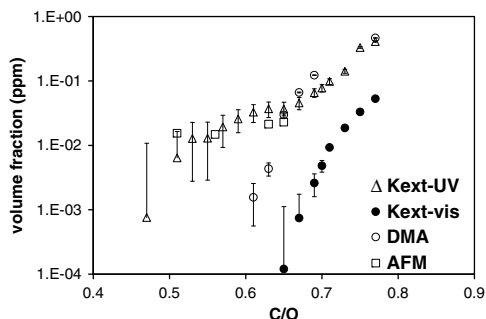


Fig. 8. Volume fraction of total particles determined by (Δ) UV-absorption, (\bullet) visible-absorption, (\circ) DMA and (\square) AFM measured at 10 mm in ethylene/air flames with different C/O ratios.

For the examined flame conditions the soot formation threshold, defined as the C/O value where light absorption in the visible is detected, is at 0.67. The onset of nanoparticles by optical measurements can be considered to be the condition in which the measured scattering signal, Q_{vv} , or light absorption and fluorescence in the UV start to noticeably increase above the gas phase background. Below $C/O = 0.5$ data uncertainty is too large to detect the presence of particles. The volume fractions determined by AFM measurements are in close agreement with the optical measurements when AFM results are corrected for the particle sticking efficiency.

The main difference between the measurements in Fig. 8 is that the DMA measurements show a drastic drop-off in particle volume fraction for $C/O < 0.65$, and no particles are detected by the DMA for $C/O < 0.6$ flames. This drop-off is not seen in the AFM or optical measurements, which measure a significant amount of particles in the range $C/O = 0.5$ – 0.65 . It is interesting to note that the drop-off in the concentration of nanoparticles is measured by DMA at low C/O where the size distributions show only the smallest mode ($d < 3 \text{ nm}$). Since very small particles can be easily lost during probe sampling due to their large diffusivity and consequent number of wall collisions, the disagreement of DMA measurements can be ascribed to this effect [59,60,99].

The results presented for combustion-formed nanoparticles in premixed ethylene flames can be extended to different fuels also including methane and benzene [44,100–103]. For flames burning aromatic compounds the discrimination between precursor nanoparticles and soot is not as easy as in aliphatic fuel flames. Indeed the presence of aromatic compounds already in the main oxidation zone of the flame favors growth reactions which lead to the formation of nanoparticles already in the flame front rendering measurements more difficult [103].

4. Nanoparticles in non-premixed flames

Detection of particles in co-flowing non-premixed flames is complicated by flame geometry. In spite of this disadvantage, they have been the subject of many investigations aiming to detect both soot [104–109] and its precursor particles [45–47,89,91–93] since non-premixed combustion is the regime usually encountered in practical combustion systems.

As in premixed flames, the main characteristic which distinguishes nanoparticles from soot particles is their different extinction spectra. However, the measured absorption spectra in co-flowing diffusion flames represent integrated values of the local absorption coefficients along the optical path through the flame. The integrated measurements had to be inverted in order to calculate the local spectral values by applying an onion-peeling inversion technique, which assumes the flame to be axial symmetric. This technique allows the determination of the local spectral extinction coefficients from the spectral absorption profiles obtained at different radial positions from the centre to the outer region of the flame. As for premixed flames the gas species contribution can be evaluated and subtracted from the measurements.

Spectral absorption coefficients in the range 200–500 nm have been measured in an atmospheric pressure non-smoking ethylene/air flame with an ethylene flow rate of $3.85 \text{ cm}^3/\text{s}$ [47]. Fig.

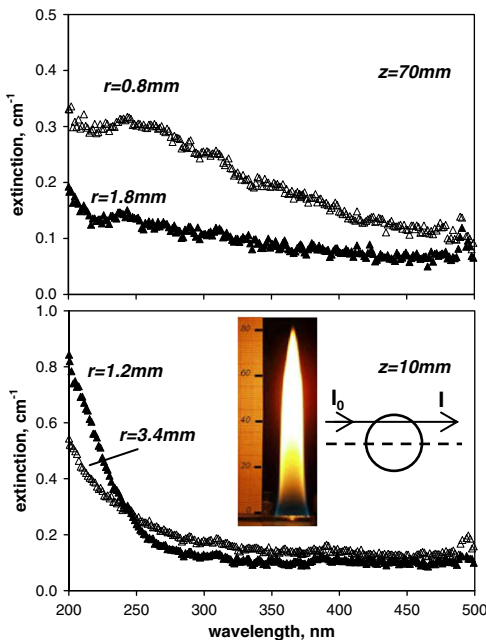


Fig. 9. Extinction measurements at 10 and 70 mm from the burner outlet of a non-smoking ethylene co-flowing diffusion flame for two radial positions.

ure 9 reports the extinction spectra at 10 and 70 mm and at two radial positions. Integrated extinction spectra measured in the lower part of the flame ($z = 10 \text{ mm}$) monotonically decrease from 200 nm to the visible where they become negligible. The shape of the spectra change completely at the tip of the flame ($z = 70 \text{ mm}$). Measurable absorption signals are observed up to the visible and a slight hump in the spectra can be seen centered at approximately 240 nm at $z = 70 \text{ mm}$.

Local extinction spectra, obtained after inversion of the integrated absorption values and corrected by the contribution of gaseous species absorption confirm the spectral behaviour. Figure 10 presents the local extinction spectra at 10 and 70 mm for two radial positions. In the lower part of the flame ($z = 10 \text{ mm}$), the extinction spectrum at $r = 1.2 \text{ mm}$ shows strong absorption in the UV which decreases at increasing wavelengths. It falls below the limit of detection for $\lambda > 300 \text{ nm}$. The lack of visible absorption at $r = 1.2 \text{ mm}$ is indicative of the absence of soot particles. This spectral form is similar to that found in premixed flames and is attributed to visible-transparent nanoparticles. At the same flame height, but far from the flame centerline ($r = 3.4 \text{ mm}$) stronger absorption in the visible appears indicating the presence of soot particles. The spectral absorption curve due to soot particles also reported in Fig. 10 was evaluated by absorption measurements performed on

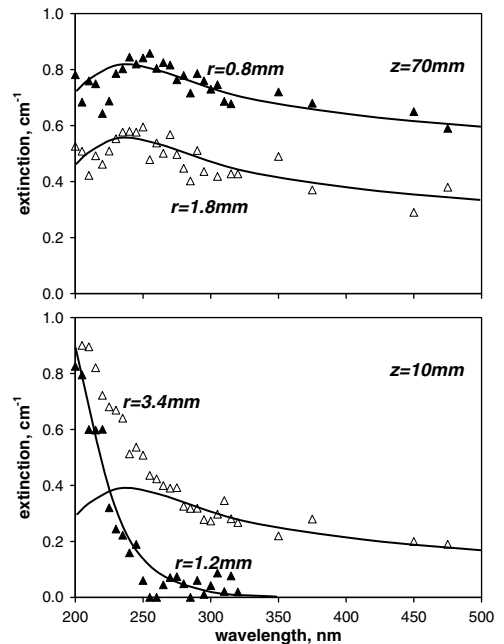


Fig. 10. Local extinction spectra at 10 mm and 70 mm from the burner outlet of a non-smoking ethylene co-flowing diffusion flame for two radial positions.

soot deposited on a quartz disk. It is clearly evident that there is an excess of absorption in the UV between 200 and 300 nm which cannot be attributed to soot particles.

The ultraviolet broadband extinction, the dominant feature in the lower part of the flame, is no longer apparent in the local extinction spectra obtained at 70 mm. The spectra measured at this axial location are mainly due to soot particles, as shown by the soot absorption spectrum reported in the upper part of Fig. 10 for comparison.

Following the same procedure used for pre-mixed flames, the volume fractions of nanoparticles and soot have been derived from absorption measurements in the UV and in the visible. Figure 11 reports the volume fractions of soot and visible-transparent particles at 10, 30 and 50 mm evaluated from absorption measurements as a function of the radial position. In the same Figure the radial temperature profiles are also shown to distinguish the different flame zones in which particles are formed.

Nanoparticles and soot are measured in comparable concentrations but in different flame regions. Nanoparticles are preferentially formed in the lower temperature flame regions and closer to the flame axis. Soot is present in a narrow annular region closer to the maximum flame temperature zone and its maximum volume fraction is measured just after the decrease of nanoparticle volume fraction. The radial position of the maximum soot volume fraction shifts, at increasing heights, towards the flame centerline reaching the flame axis at the tip.

Scattering, with the contribution from gaseous products subtracted, has been used for the determination of mean particle size. Size estimation of nanoparticles can only be made in flame regions with negligible soot. Indeed because the quantity determined by the measurements is the high moment ratio d_{63} , the method is biased to the large diameters of soot particles in the wings of the flame which obscure the contribution of nanoparticles to the scattering signal. Mean particle diameters (d_{63}) are reported in Fig. 12 as a function of radial position. Particle diameters of about 3–4 nm are measured at $z = 10$ mm and have typical sizes of nanoparticles as measured in premixed flames (Fig. 3). The build-up of the scattering signal at greater heights corresponding with soot formation correlates with the increase of the mean size of the particles due to the presence of both nanoparticles and larger soot particles. At higher flame heights, where soot formation extends to the whole flame and moves from the flame wings to the centerline, the measured mean particle size reaches values of the order of 50 nm which are typical values of soot particles measured in such flames.

Spectral LIF and LII have supported the extinction measurements. LIF spectra show two

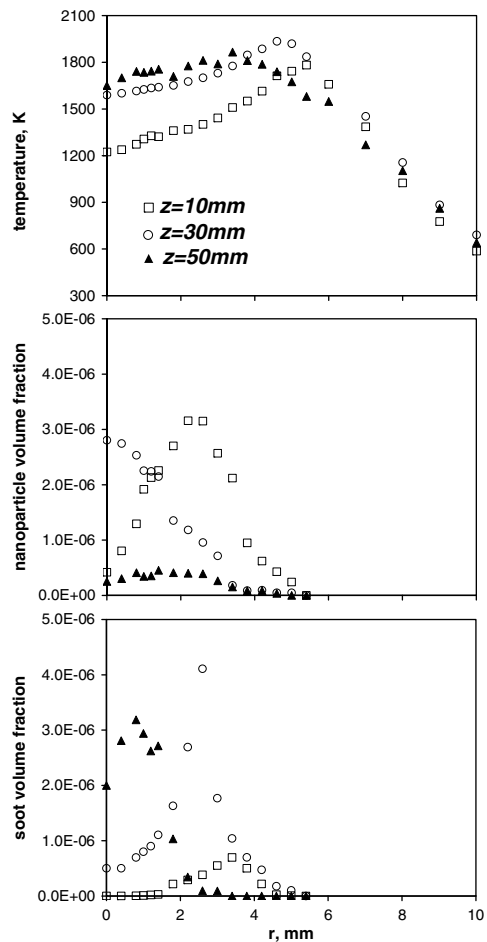


Fig. 11. Radial distribution of volume fractions of soot and nanoparticles at selected axial positions in the non-smoking ethylene co-flowing diffusion flame, and corresponding temperature profiles.

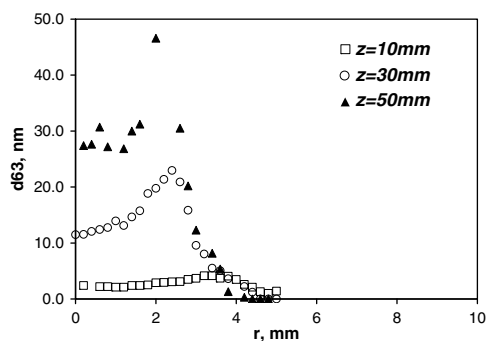


Fig. 12. Evolution of the mean particle diameters, d_{63} , at selected axial positions in the non-smoking ethylene co-flowing diffusion flame.

broadband peaks: the first in the UV at 330 nm and the second shifted in the visible at 440 nm. Moving from the fuel side towards the flame reaction zone the fluorescence intensity decreases whereas the incandescence of soot particles increases. Approaching the maximum temperature region LII also decreases due to the oxidation of the soot particles. Figure 13 reports fluorescence at 330 nm and LII signals measured at 10 and 30 mm along the flame axis. The LIF and LII signals show the same behavior as the volume fraction profiles of nanoparticles and soot reported in Fig. 11 which have been determined by spectral absorption measurements.

Thermophoretic probing conducted on the same flame along the radial direction at $z = 10, 20$ and 30 mm has revealed the existence of nanoparticles on the fuel side of the reaction zone [89]. Nanoparticles appeared quite “transparent” on the fuel side, more opaque near the luminosity front and small, highly opaque near the reaction zone. They are formed in the same region where fluorescence is measured suggesting that they are composed of fluorescing aromatics.

The smallest observable nanoparticles by TEM were estimated to be 3 nm diameter in excellent agreement with the optical results. Mass spectrometric analyses [91] of nanoparticle samples in the fuel-side of diffusion flames showed the prominence of the benzenoid PAH in the mass range of

202–300 u supporting the aromatic nature of nanoparticles.

A counter-flow flame configuration is more suitable for the study of particle formation in non-premixed conditions since data interpretation is not influenced by the interference of particle trajectories, as occurs in coflowing flames.

Spectral absorption and LIF and LII measurements have been performed in a sooting counter-flow flame of ethylene/air [46,110]. The fuel and oxidant flow rates are such that the main oxidation and the soot formation zones are located on the oxidizer side. In this way soot particles are transported away from the flame front towards the stagnation plane avoiding particle oxidation [111,112]. Figure 14 reports, in the upper part, the volume fractions of UV absorbing species and soot as determined by absorption coefficients in the UV at 266 nm and in the visible at 532 nm. Three regions in the flame can be observed. Moving from the fuel side, UV absorbing species are detected across the stagnation plane of the flame which is located at about 4.2 mm (reported as a dashed line in the Figure). This zone is characterized by a low temperature of the order of 700–1100 K. To the right of the stagnation plane, visible absorption is detected which decreases moving towards the flame front, which is located at about 8 mm. Between the maximum visible absorption and the flame front a second peak of UV absorbing species is measured. In this latter region the temperature is higher than 1300 K and oxidation and pyrolysis overlap.

The different flame regions also show different laser induced emissions. Figure 14 (intermediate part) reports the fluorescence signals detected at 350 and 440 nm and the LII along the flame. The flame zone across the stagnation plane, which is characterized by UV-absorption attributable to nanoparticles, also shows UV-fluorescence at 350 and 440 nm. The zone where visible absorption attributable to soot particles is detected is characterized by incandescence whereas the region closer to the flame front in which a second peak of UV absorbing species is present shows again UV fluorescence but now mainly at 350 nm.

Different fluorescence signals in the nanoparticle region seems to indicate that two classes of nanoparticles are formed. They have quite the same size but different chemical properties.

Figure 14 (lower part) also reports the estimated number concentration and particle mean size considering optical properties of the particles as for premixed flames. In the fuel side of the flame nanoparticles with mean sizes of the order of 3–4 nm are formed in large number concentrations. Their number concentration decreases as the particle size increases in the region of soot formation. A second nucleation zone is observed in the high temperature region closer to the flame zone where particles again show smaller sizes, about 5 nm.

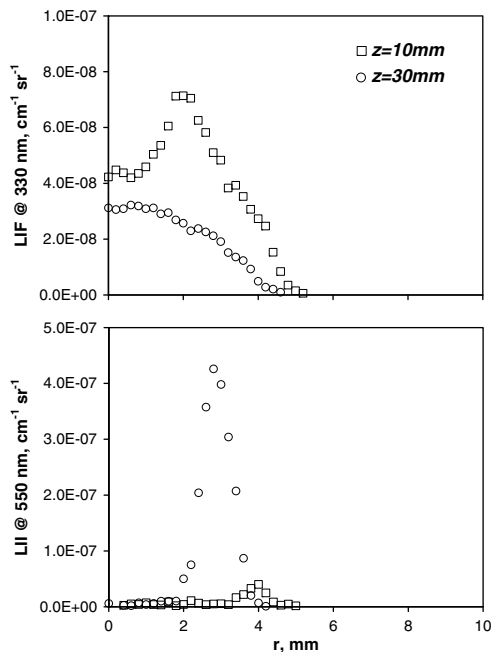


Fig. 13. Laser induced fluorescence at 330 nm and laser induced incandescence at 550 nm at selected axial positions in the non-smoking ethylene co-flowing diffusion flame.

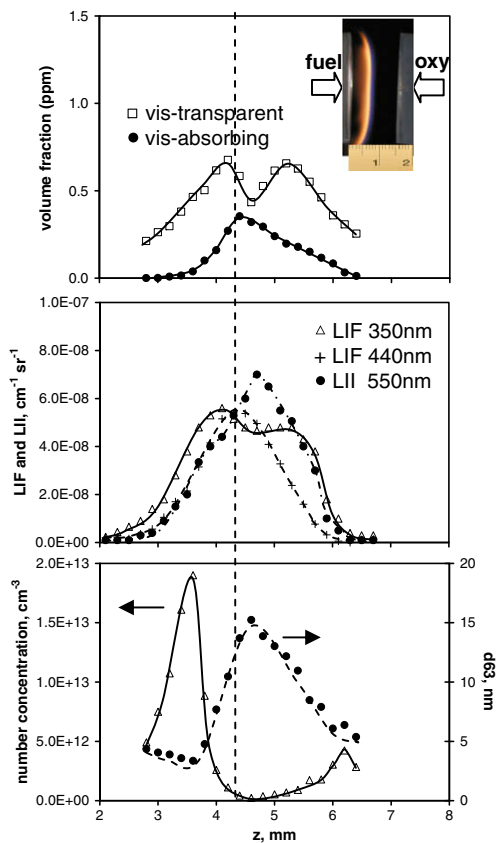


Fig. 14. Volume fractions of visible-absorbing and visible-transparent particles (upper), LIF at 350 and 440 nm and LII at 550 nm (intermediate) and number concentration and mean sizes of the particles (lower) measured in a counter-flow diffusion flame of ethylene.

The use of constant optical properties for nanoparticles is questionable in view of the different fluorescence characteristics in the two flame zones.

AFM measurements performed on samples collected by thermophoresis on a mica disk inserted parallel to the streamlines in the flame support the optical measurements [110]. Figure 15 reports the particle size distributions measured in the fuel side close to the stagnation plane, in the region between the stagnation plane and the flame front and close to the flame front. Particles detected in the fuel side close to the stagnation plane have sizes of about 2–3 nm, are transparent to visible radiation and exhibit UV and visible fluorescence suggesting that these particles are the result of PAH physical coagulation which is favored at low temperatures. The fluorescence spectra detected in this region of the flame are similar to those of PAH excimers. Particles detected on the right side of the stagnation plane before the flame zone have a bimodal size distribution with a first mode at 5 nm due to UV-fluo-

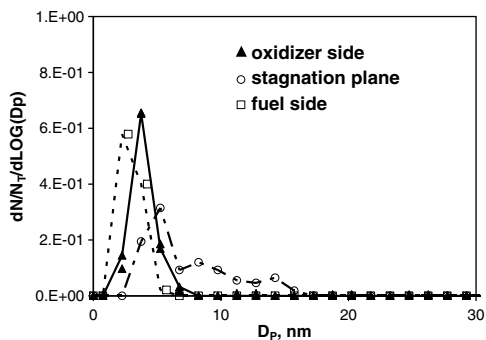


Fig. 15. Particle size distribution measured by AFM in the oxidizer side (\blacktriangle), across the stagnation plane (\circ) and in the fuel side (\square) of a counter-flow diffusion flame of ethylene.

rescing nanoparticles and a second mode due to soot. In the region close to the flame front where the temperature is relatively high and radicals are abundant, particles again have a modal size distribution with a maximum at 3–4 nm. These particles behave spectroscopically like the isolated gas-phase PAHs of which they are comprised and which exhibit fluorescence far into the UV [46]. They can be formed by reactive coagulation which leads to the formation of aromatic species with a maximum of 2–3 ring chromophores connected by sp^3 bonding similar to those found in premixed flames.

The results presented have shown that combustion-formed nanoparticles in non-premixed flames have some characteristics already found in premixed flames but also have some peculiarities. Indeed the presence of low-temperature regions with high concentrations of fuel and pyrolysis products such as PAHs can favor the nucleation of nanoparticles through a physical coagulation mechanism which leads to PAH stacks held together by weak van der Waals-forces. These nanoparticles have sizes similar to those of nanoparticles found in premixed flames but have a different chemical nature; they do not contain oxygen since they are formed in the fuel side of the flame and hence they might have less interaction with water and biological systems. Nanoparticles with the same size and chemical structure of those found in premixed flames are also formed in the region between the flame front and the soot formation region. The presence of these two classes of nanoparticles has been well observed in counter-flow flames.

5. Nanoparticles emitted from practical combustion devices

Small nanoparticles emitted from practical combustion devices are often considered not to

be directly connected with combustion, but rather thought to nucleate during dilution and cooling of the exhausts [113,114]. However, many of the features of the combustion-formed nanoparticles in laboratory studies may have pertinence to the emission from practical systems.

Figure 16 shows the particle size distribution functions by number measured with AFM and DMA at the exhausts of gasoline and diesel powered vehicles operated on a dynamometer [86,115]. The particle size distribution emitted by a diesel engine shows two particle modes similar to those observed in premixed flames (Figs. 5 and 6): nano-sized and soot particles. By contrast the gasoline vehicle exhaust shows only the first mode due to nanoparticles. Optical measurements have also been performed at the exhausts of the two vehicles showing extinction spectra similar to those measured in flames [21,86]. There is also rather good agreement between the relative amounts of nanoparticles and soot determined by UV-visible extinction and by AFM measurements at the vehicle exhausts [86]. The similarity in size and extinction spectra suggests that nanoparticles measured in vehicle exhaust are generated in the combustion chamber and both nanoparticles and soot modes survive the exhaust system without significant growth.

The concentrations of high-molecular-mass tar-like species and soot during the combustion cycle in a single-cylinder direct injection diesel-

engine were measured in a pioneering work by Ciajolo and co-workers [116–118]. Samples were withdrawn with a fast in-cylinder gas sampling device during the combustion cycles and were analysed. They found that the formation of high-molecular-mass tar-like species occurs just after fuel ignition and precedes soot formation. The chemical characterization of the sampled species showed the presence of PAHs and aromatic compounds of high molecular mass exhibiting absorption and fluorescence in the UV similar to those found in laboratory flames. Extinction and scattering measurements performed in the combustion chamber of a “transparent” diesel engine have further confirmed the in-cylinder formation of nanoparticles during diesel combustion [119]. Recently, Kubo [120] measured the in-cylinder size distribution of the particles formed during the diesel cycle with a DMA and found a unimodal particle size distribution with a peak at about 3 nm in the earlier stage of combustion, which moved from around 3–7 nm during combustion. As combustion proceeded a second mode became clearly distinct at about 20 nm. Mass spectrometric analysis, AFM and TEM measurements characterized the sampled material. It was concluded that nearly planar PAHs grow up to form agglomerates of the dimers and trimers of the planar molecules, a few nanometers in diameter. Soot particles emitted from the engine, however, have like-crossed structures thus showing that particulate nanostructures change greatly in the engine combustion process and even in the exhaust manifold. Data by Kubo strongly support the hypothesis that the combustion process contributes to the emission of particles from engines although the contribution of sulphur compounds and volatile organic compounds to particle nucleation during dilution and cooling of the exhausts can not be excluded.

In order to assess the role of combustion rather than that of fuel characteristics on the emission of nanoparticles from practical devices, measurements of particle size distributions were made at the exhausts of a cook stove and of a burner for home appliances, both fuelled with methane. Figure 17 reports the size distribution functions determined by DMA [121,122]. The cook stove has a non-premixed flame structure whereas the burner for home appliances is more like a premixed flame. In both cases the particle size distributions only show a modal diameter at 2–4 nm. In these experiments the contribution of volatile organic compounds from the unburned fuel can be excluded since methane is used. Optical measurements were also made at the exhaust of these combustion systems showing similarity of properties of flame generated nanoparticles with those emitted from methane fuelled burners.

The observation that particulate matter in combustion emissions has the same size and opti-

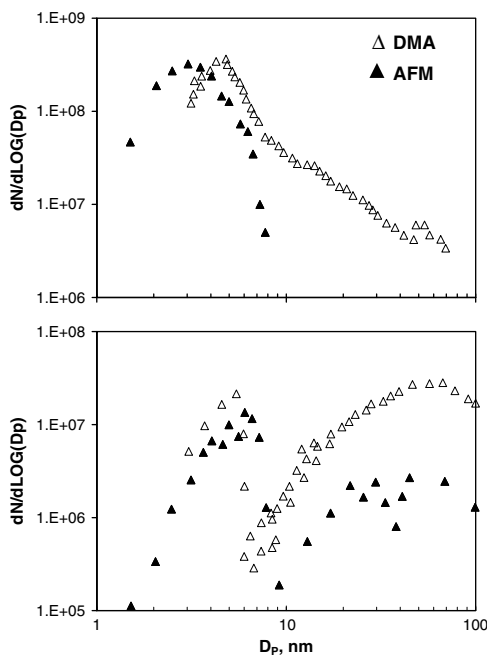


Fig. 16. Particle size distribution measured by AFM (\blacktriangle) and DMA (\triangle) at the exhaust of a gasoline (upper) and a diesel (lower) vehicle.

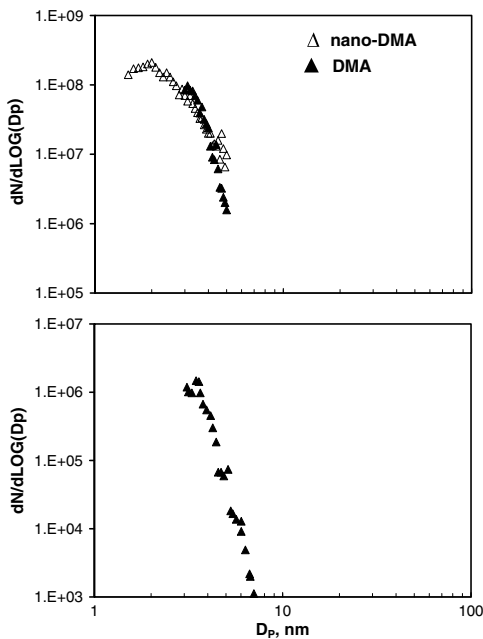


Fig. 17. Particle size distribution measured by DMA (Δ , \blacktriangle) at the exhaust of a cook stove (upper) and a burner for home appliances (lower).

cal properties of flame-generated nanoparticles implies that nanoparticle emission can be generally related to combustion as well as to nucleation during dilution and cooling in the exhaust. However, if nanoparticles are a concern for the atmosphere and on human health, then spark-ignition and methane-fuelled combustion systems as well as diesel engines may be important sources.

6. Modelling aspects

Modelling of particle formation in combustion environments has received great attention in recent years [123–125]. Models, today, are able to simulate the concentration and size distributions of particles in many combustion systems including laminar premixed and diffusion flames [55,126–132]. Even some attempts to model particle formation in turbulent flames have shown that detailed kinetic models show encouraging progress for complex systems [133].

In early reaction models, soot particles were considered as the mass accumulated in aromatic species above a certain molecular mass [134]. This approximation accounts for the amount of soot mass formed, but particle size is not considered. The transition from gas-phase to particles is considered essentially a kinetic process and no effects of particle growth and coagulation is considered.

In follow-up work, the model of nucleation is expanded: PAH of some sizes begin to stick to each other during collision, thus forming PAH dimers. PAH dimers collide with PAH molecules forming PAH trimers and so on. Pyrene was considered the first aromatic species in the PAH series able to form stable dimers at flame temperatures and the dimers were considered as the first soot nuclei. Surface addition mainly by acetylene was responsible for soot loading [124,135].

Models which combine dimerization of PAHs with the formation of ring-ring aromatic species through a purely-chemical mechanism have recently been proposed [126–129]. The growing molecular species acquire the properties of a condensed phase. Surface reactions with gas-phase species, mainly acetylene and PAHs, and coagulation of the particles determine their final concentration and size distribution. Surface growth is based on chemical analogy of gas-phase aromatic chemistry.

Two different approaches have been used to couple gas-phase chemistry with aromatic growth mechanisms: the method of moments [135–138] and the discrete sectional method [128,129,139,140].

In the method of moments, the detailed description of particle dynamics is modelled in terms of moments of the particle size distribution (PSD) function. Knowledge of the infinite set of these moments is equivalent to knowledge of PSD itself. The first few PSD function moments are however sufficient for determination of particle properties, such as volume fraction, mean particle size and variance of the PSD function. If only a few moments are considered a functional form for the PSD function has to be assigned. The method of moments was recently extended to include agglomeration of soot particles into fractal aggregates and the determination of active sites on particle surface [141,142].

In the discrete-sectional method, the ensemble of aromatic compounds with molecular mass higher than the largest aromatic compounds in the gas-phase is divided into classes of different molecular mass and all reactions are treated in the form of gas-phase chemistry using compound properties such as mass, numbers of carbon and hydrogen atoms averaged within each section. The molecular mass distribution of the species is obtained from the calculation and is not hypothesized a priori. Particle evolution is followed by combining the laws of reacting flows with the population balance for suspended particles.

These models have been used to predict the volume fractions of particles and their size distribution functions in a variety of flame conditions [127–129]. The coupling of the physical and chemical routes for molecular weight growth makes it possible to follow particle nucleation in a wider range of conditions including slightly-sooting flames and non-premixed flames. Results appear

to correctly reproduce the size distribution of nanoparticles in non-sooting flames and the development toward bimodal particle size distributions when soot is formed [129].

The different C/O ratio and temperature fields encountered in the flame environments may determine the relative importance of the two main processes of particle growth: the purely-chemical growth and the physical dimerization pathway. Flame zones characterized by high temperature and large radical concentrations should favor the chemical growth mechanism, i.e. the addition of aromatic molecules to aromatic radicals. On the other hand, lower temperatures and a lack of radicals should favor the physical growth of the particles through a coagulation process.

The relative importance of the two processes can be evaluated as a function of flame temperature and radical concentration in the flames.

The purely-chemical growth can be schematized by:



where A_i is a species belonging to the i^{th} section and A_i^* its radical form. The chemical-growth rate depends on the amount of the aromatic species relative to the stable species. Assuming steady-state for radicals, the rate of aromatic growth can be expressed as:

$$\text{rate chemical growth} = k_2[A_i]^2 K_{\text{eq}}[H]/[H_2]$$

where K_{eq} is the equilibrium constant of rx.1. Consequently the rate of aromatic growth depends on both temperature and $[H]/[H_2]$ in the flame environment.

The physical dimerization pathway can be schematized by:



The rate of rx.3 can be expressed as:

$$\text{rate physical growth} = k_3[A_i]^2$$

Both constants k_2 and k_3 depend strongly on temperature, but in opposing ways; k_2 follows the Arrhenius formulation and increases for increasing temperatures

$$k_2 = k_{02} * \exp(-Ea_2/RT)$$

whereas k_{02} is the pre-exponential factor and Ea_2 the activation energy of rx.2.

The physical dimerization pathway constant k_3 is the product of the gas-kinetic collision constant (k_{GK}) and the sticking efficiency of the colliding particles:

$$k_3 = k_{\text{GK}} * \gamma$$

It decreases as temperature increases because of the decrease of sticking coefficient given by the expression [90,143]:

$$\gamma = 1 - (1 + \Phi_0/RT) \exp(-\Phi_0/RT)$$

where Φ_0 is the minimum of the interaction potential for the colliding particles and R is the universal gas constant.

Ratio of the rates of the physical and the chemical growth can be expressed as:

$$\frac{\text{rate physical growth}}{\text{rate chemical growth}} = \frac{k_{\text{GK}}(1 - (1 + \Phi_0/RT) \exp(-\Phi_0/RT))}{k_{02} \exp(-Ea_2/RT) K_{\text{eq}}[H]/[H_2]}$$

At lower temperatures and $[H]/[H_2]$, rate of particle growth by physical coagulation becomes dominant. This regime is observed in the post-flame zone of very-rich laminar premixed flames and in the fuel side of diffusion flames. In the preheat zone of premixed flames, the lower temperature which promotes physical coagulation is counterbalanced by the high $[H]/[H_2]$ which favor the purely-chemical growth. Just downstream of the flame front of rich flames, the higher temperatures and higher $[H]/[H_2]$ promote purely-chemical growth.

Figure 18 reports as a line the values of $[H]/[H_2]$ vs temperature where the rates of the physical and the chemical routes are equal. It has been calculated considering molecular particles with mass of the order of 1000 u, a Hamacker constant of $5 \cdot 10^{-20} \text{J}$ for the interaction potential [90] and an activation energy for rx.2 of 15000 cal/mol [129]. The region above the line is the $[H]/[H_2]$ vs temperature domain where particle growth is dominated by purely-chemical growth whereas the region below the line is where the physical route is dominant. Typical modelled values of $[H]/[H_2]$ at temperature conditions encountered in premixed flames of various hydrocarbons are reported in the upper part of Fig. 18 whereas the lower part of Fig. 18 reports the same data for non-premixed flames.

In not-fully sooting premixed flames the values of $[H]/[H_2]$ and temperature encountered along the flame axis lie mainly where the chemical growth mechanism prevails over the coagulation route (Fig. 18 – upper). Only in fully-sooting flames does the coagulation process prevail, but only in the post-flame zone.

In non-premixed flames both conditions which favor chemical over physical mechanisms can be encountered (Fig. 18 – lower). Physical coagulation is prevalent in the fuel region of the flames, characterized by lower temperatures and lower radical concentrations. Chemical growth mechanism occurs closer to the flame reaction zone, characterized by higher temperatures and radical concentrations.

This simple analysis illustrates how the growth of aromatics and the chemical nature of the particles depend on local regimes of temperature and radical concentrations. Stacked PAHs are formed

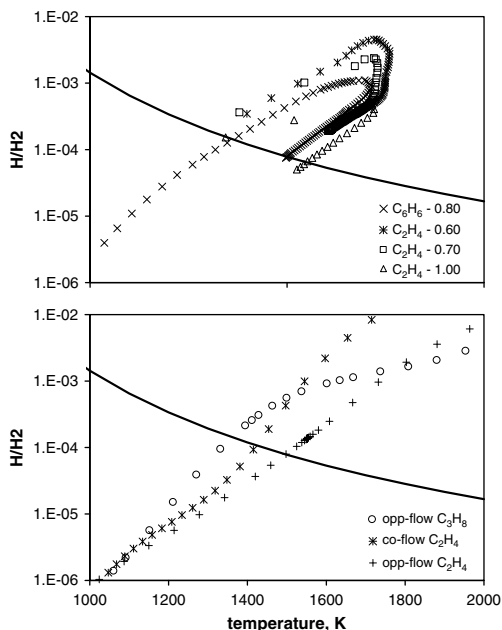


Fig. 18. Modelled values of $[H]/[H_2]$ vs temperature where the rates of the physical and the chemical routes are equal (lines). Points represent typical modelled values of $[H]/[H_2]$ and temperature conditions encountered in premixed (upper) and diffusion flames (lower).

if the physical dimerization occurs while aromatic-aliphatic linked species formation occurs if purely-chemical growth occurs. It would be interesting to extend this analysis to the role of oxygen molecules and hydroxyl radicals which might influence the chemical and physical routes in a different manner.

7. Conclusions

Combustion of fossil fuels produces carbonaceous nanoparticles both in premixed and non-premixed flame conditions. Two classes of carbonaceous material are mainly formed in combustion: nanoparticles with sizes in the range 1–5 nm, and soot particles, with sizes from 10 to 100 nm. Chemical and spectroscopic analysis give an indication of the chemical nature of the particles and show that the smaller particles can be thought as staked PAH structures or polymer-like structures containing sub-units with aliphatic and aromatic bonds and occasionally oxygen, depending on the flame environment. Staked PAH structures are formed if physical molecular growth mechanism, based on PAH dimerization, is favored by low temperatures and low radical concentrations. On the other hand, aromatic-aliphatic linked structures are formed when chemical-growth mechanism is enhanced, i.e. higher

temperatures and higher radical concentrations. Oxidative-pyrolytic conditions, typical of fuel-rich, premixed flames, favor the latter mechanism while purely-pyrolytic conditions, typical of the fuel side of diffusion flames, favor the aromatic dimerization.

The process of soot formation is the coagulation of the 1–5 nm particles, which at the same time add compounds from the gas-phase and lose H, gaining a higher condensed-ring aromatic or graphitic structure.

Nanoparticles are also found in the exhaust of practical combustion systems. This has been mainly attributed to condensation of low volatility hydrocarbons during dilution and cooling of the exhausts. However, the similarity of the chemical properties and the size distribution functions of the emitted particles with those found in laboratory flames suggests that combustion-formed nanoparticles can escape the combustion process and be emitted into the atmosphere. Thus combustion, as well as the fuel, may have a dominant role in determining the type and amount of particles emitted.

Nanoparticles are present in low mass concentration, but surprisingly high number concentrations due to their very low sizes. The emission of these particles into the atmosphere constitutes a serious concern for health and for their contribution to photochemical smog. The smallest particles play a particularly important role in health since they are able to penetrate deeper than larger particles into the respiratory system. They may also affect the radiation balance of the atmosphere by serving as condensation nuclei for cloud formation and for contrails in the upper atmosphere. For these reasons, the role of combustion-formed nanoparticles is of central interest in the field of atmospheric chemistry. These particles may account for a large part of the organic carbon in urban atmospheres and they might also explain the phenomenon of “nucleation burst” after agglomeration in rain.

Nanoparticles have low coagulation rates at flame temperatures. This interesting behavior may explain why they escape exhaust systems without significant growth at high temperature. The low coagulation rate is due to the weak van der Waals-interactions between particles relative to their thermal energy and it may also be related to the chemical nature of the particles. Functional groups containing oxygen have been found in nanoparticles. If oxygen containing functionalities are present in combustion-generated nanoparticles, it is also possible to explain why nanoparticles with sizes below 3 nm remain dispersed in water samples in contrast to larger and more graphitic soot particles. The presence of oxygen in nanoparticles is of great importance and it may also play a role in how these particles affect biological systems.

The low coagulation rate of nanoparticles means that some of them survive for a long time. They undergo atmospheric reactions and they can also spread to areas without particle emissions making nanoparticles emitted from combustion systems a global problem [144].

Acknowledgments

I express my appreciation for the support of the late Professor Antonio D'Alessio who initiated so much of the combustion research in Napoli. I also thank Dr. P. Minutolo of Istituto Ricerche sulla Combustione, CNR, Napoli and Professor John Kent of the University of Sydney and LeeAnn Sgro of the University of Napoli for helpful discussions. My thanks to our PhD students Mario Commodo, Francesco Carbone, Mariano Sirignano, Andrea De Filippo and Annalisa Bruno for their modelling and experimental work.

I am particularly grateful to Dr. Anna Ciajolo of Istituto Ricerche sulla Combustione, CNR in Napoli for her helpful suggestions and for the stimulating discussions we have shared over the years.

References

- [1] G. Oberdörster, E. Oberdörster, J. Oberdörster, *Environ. Health Perspect.* 113 (2005) 823.
- [2] T. Osunsanya, G. Prescott, A. Seaton, *Occup. Environ. Med.* 58 (2000) 154.
- [3] I. Kennedy, *Proc. Combust. Inst.* 31 (2) (2007) 2757.
- [4] B. Karcher, *Survey Geophys.* 20 (2) (1999) 113.
- [5] A.L. Robinson, N.M. Donahue, M.K. Shrivastava, et al., *Science* 315 (2007) 1259.
- [6] B.J. Turpin, P. Saxena, E. Andrews, *Atmos. Environ.* 34 (2000) 2983.
- [7] Y.J. Kaufman, R.S. Fraser, *Science* 277 (1997) 1636.
- [8] B.J. Finlayson-Pitts, J.N. Pitts Jr., *Science* 276 (1997) 1045.
- [9] B.S. Haynes, H.Gg. Wagner, *Prog. Energy Combust. Sci.* 7 (1981) 229.
- [10] J.B. Howard, *Proc. Combust. Inst.* 23 (1990) 1107.
- [11] J.S. Lighty, J.M. Veranth, A.F. Sarofim, *J. Air Waste Manage. Assoc.* 50 (2000) 1565.
- [12] R.A. Dobbins, *Aerosol Sci. Technol.* 41 (2007) 485.
- [13] D.C. Siegla, G.W. Smith (Eds.), *Particulate Carbon Formation During Combustion*, Plenum Press, New York, 1981.
- [14] J. Lahaye, G. Prado (Eds.), *Soot in Combustion Systems and Its Toxic Properties*, Plenum Press, New York, 1983.
- [15] H. Jander, H. Gg. Wagner (Eds.) *Soot Formation in Combustion – an International Round Table Discussion*, Vandenhoeck and Ruprecht, Göttingen, 1990.
- [16] H. Bockhorn (Ed.), *Soot Formation in Combustion*, Springer, Berlin-Heidelberg-New York, 1994.
- [17] A.F. Sarofim, A. D'Anna, H. Wang (Eds.) *International Workshop on Combustion Generated Fine Carbon Particles*, Villa Orlandi, Italy, May 13–16, 2007.
- [18] A. D'Alessio, in: D.C. Siegla, G.W. Smith (Eds.), *Particulate Carbon Formation During Combustion*, Plenum Press, New York, 1981, pp. 207–256.
- [19] A. D'Alessio, A. D'Anna, A. D'Orsi, P. Minutolo, R. Barbella, A. Ciajolo, *Proc. Combust. Inst.* 24 (1992) 973.
- [20] A. D'Alessio, A. D'Anna, G. Gambi, P. Minutolo, *J. Aerosol Sci.* 29 (1998) 397.
- [21] A. Borghese, S.S. Merola, *Proc. Combust. Inst.* 27 (1998) 2101.
- [22] P. Minutolo, G. Gambi, A. D'Alessio, S. Carlucci, *Atmos. Environ.* 33 (1999) 2725.
- [23] A. D'Anna, A. D'Alessio, P. Minutolo, in: H. Bockhorn (Ed.), *Soot Formation in Combustion: Mechanisms and Models*, Springer-Verlag, Berlin, 1994, pp. 83–103.
- [24] J. Jensen, R.D. Guettler, J.L. Lyman, *Chem. Phys. Lett.* 277 (1997) 356.
- [25] T. Joutsenoja, A. D'Anna, A. D'Alessio, M.I. Nazzaro, *Appl. Spect.* 55 (2001) 130.
- [26] E. Clar, *Polycyclic Hydrocarbons*, Academic Press, London, 1964.
- [27] J.B. Birks, *Photophysics of Aromatic Molecules*, Wiley, London, 1970.
- [28] I.B. Berlman, *Handbook of Fluorescence Spectra of Aromatic Molecules*, Academic Press, New York, 1971.
- [29] C.J. Dasch, *Proc. Combust. Inst.* 20 (1984) 1231.
- [30] L.A. Melton, *Appl. Optics* 23 (1984) 2201.
- [31] S. Will, S. Schraml, A. Leipertz, *Optics Lett.* 20 (1995) 2342.
- [32] P. Roth, A.V. Filippov, *J. Aerosol Sci.* 27 (1996) 95.
- [33] A.V. Filippov, M.W. Markus, P. Roth, *J. Aerosol Sci.* 30 (1999) 71.
- [34] R.J. Santoro, C.R. Shaddix, in: K. Kohse-Höinghaus, J.B. Jeffries (Eds.), *Applied Diagnostics*, Taylor and Francis, New York-London, 2002, p. 252.
- [35] T. Lehre, B. Jungfleisch, R. Suntz, H. Bockhorn, *Appl. Optics* 42 (12) (2003) 2021.
- [36] D.S. Coe, J.I. Steinfeld, *Chem. Phys. Lett.* 76 (1980) 485.
- [37] D.S. Coe, B.S. Haynes, J.I. Steinfeld, *Combust. Flame* 43 (1981) 211.
- [38] A. Leipertz, F. Ossler, M. Aldén, in: K. Kohse-Höinghaus, J.B. Jeffries (Eds.), *Applied Diagnostics*, Taylor and Francis, New York-London, 2002, p. 359.
- [39] R.L. Vander Wal, *Proc. Combust. Inst.* 26 (1996) 2269.
- [40] J.H. Miller, W.G. Mallard, K.C. Smyth, *Combust. Flame* 47 (1982) 205.
- [41] A. Ciajolo, A. Tregrossi, R. Barbella, R. Ragucci, B. Apicella, M. de Joannon, *Combust. Flame* 125 (4) (2001) 1225.
- [42] A. Ciajolo, R. Ragucci, B. Apicella, R. Barbella, M. de Joannon, A. Tregrossi, *Chemosphere* 42 (5–7) (2001) 835.
- [43] F. Beretta, V. Cincotti, A. D'Alessio, P. Menna, *Combust. Flame* 61 (1985) 211.
- [44] P. Minutolo, G. Gambi, A. D'Alessio, A. D'Anna, *Combust. Sci. Technol.* 101 (1–6) (1994) 309.

- [45] A. D'Anna, M. Commodo, S. Violi, C. Allouis, J. Kent, *Proc. Combust. Inst.* 31 (2007) 621.
- [46] A. D'Anna, M. Commodo, M. Sirignano, P. Minutolo, R. Pagliara, *Proc. Combust. Inst.* 32 (2009) 793–801.
- [47] A. D'Anna, A. Rolando, C. Allouis, P. Minutolo, A. D'Alessio, *Proc. Combust. Inst.* 30 (2005) 1449.
- [48] A. Bruno, C. de Lisio, P. Minutolo, *Optics Express* 13 (2005) 5393.
- [49] A. Bruno, C. de Lisio, P. Minutolo, A. D'Alessio, *J. Opt. A: Pure Appl. Opt.* 8 (2006) S578.
- [50] A. Bruno, F. Ossler, C. de Lisio, P. Minutolo, N. Spinelli, A. D'Alessio, *Optics Express* 16 (8) (2008) 5623.
- [51] K. Kohse-Höinghaus, *Prog. Energy Combust. Sci.* 20 (1994) 203.
- [52] A. Lamprecht, W. Eimer, K. Kohse-Höinghaus, *Combust. Flame* 118 (1–2) (1999) 140.
- [53] K. Kohse-Höinghaus, J.B. Jeffries (Eds.), *Applied Combustion Diagnostics*, Taylor & Francis, New York, 2002.
- [54] B. Zhao, Z. Yang, J. Wang, M.V. Johnston, H. Wang, *Aerosol Sci. Technol.* 37 (2003) 611.
- [55] B. Zhao, Z. Yang, M.V. Johnston, et al., *Combust. Flame* 133 (2003) 173.
- [56] M.M. Maricq, *Combust. Flame* 137 (2004) 340.
- [57] B. Zhao, Z. Yang, Z. Li, M.V. Johnston, H. Wang, *Proc. Combust. Inst.* 30 (2005) 1441.
- [58] M. Thierley, H.-H. Grotheer, M. Aigner, et al., *Proc. Combust. Inst.* 31 (2007) 639.
- [59] L.A. Sgro, A. De Filippo, G. Lanzuolo, A. D'Alessio, *Proc. Combust. Inst.* 31 (2007) 631.
- [60] P. Minutolo, A. D'Anna, A. D'Alessio, *Combust. Flame* 152 (1–2) (2008) 287.
- [61] J.C. Bordini, *Prog. Energy Combust. Sci.* 3 (1977) 151.
- [62] K.-H. Homann, *Agnew. Chem.* 37 (1998) 2434.
- [63] K.-H. Homann, in: H. Bockhorn (Ed.), *Soot Formation in Combustion*, Springer-Verlag, Berlin, 1994, p. 300.
- [64] J. Ahrens, A. Keller, R. Kovacs, K.-H. Homann, *Ber. Bunsen Ges. Phys. Chem.* 102 (1998) 1823.
- [65] K.-H. Homann, H.Gg. Wagner, *Proc. Combust. Inst.* 11 (1967) 371.
- [66] M. Bachmann, W. Wiese, K.-H. Homann, *Proc. Combust. Inst.* 26 (1996) 2259.
- [67] H.-H. Grotheer, H. Pokorny, K.-L. Barth, M. Thierley, M. Aigner, *Chemosphere* 57 (2004) 1335.
- [68] P.T.A. Reilly, R.A. Gieray, W.B. Whitten, J.M. Ramsey, *Combust. Flame* 122 (2000) 90.
- [69] J. Happold, H.-H. Grotheer, M. Aigner, *Rapid Commun. Mass Spectrom.* 21 (2007) 1247.
- [70] R. Barbella, A. Ciajolo, A. D'Anna, *Fuel* 68 (6) (1989) 690.
- [71] F.W. Lam, J.B. Howard, J.P. Longwell, *Proc. Combust. Inst.* 22 (1989) 323.
- [72] A. Ciajolo, A. D'Anna, R. Barbella, *Combust. Sci. Technol.* 100 (1994) 271.
- [73] B. Apicella, A. Ciajolo, A. Tregrossi, *Anal. Chem.* 76 (7) (2004) 2138.
- [74] A. Ciajolo, R. Barbella, A. Tregrossi, L. Bonfanti, *Proc. Combust. Inst.* 27 (1998) 1481.
- [75] A. Ciajolo, A. D'Anna, R. Barbella, A. Tregrossi, A. Violi, *Proc. Combust. Inst.* 26 (2) (1996) 2327.
- [76] B. Apicella, R. Barella, A. Ciajolo, A. Tregrossi, *Chemosphere* 51 (2003) 1063.
- [77] B. Apicella, A. Ciajolo, R. Barella, et al., *Energy Fuels* 17 (2003) 565.
- [78] B. Apicella, A. Ciajolo, I. Suelves, T.J. Morgan, A.A. Herod, R. Kandiyoti, *Combust. Sci. Technol.* 174 (2002) 403.
- [79] M. Alfè, B. Apicella, R. Barbella, A. Tregrossi, A. Ciajolo, *Energy Fuels* 21 (2007) 136.
- [80] B. Apicella, A. Carpentieri, M. Alfè, et al., *Proc. Combust. Inst.* 31 (1) (2007) 547.
- [81] J.T. McKinnon, E. Meyer, J.B. Howard, *Combust. Flame* 105 (1996) 161.
- [82] G. Rusciano, G. Cerrone, A. Sasso, A. Bruno, P. Minutolo, *Appl. Phys. B: Lasers Optics* 82 (1) (2006) 155.
- [83] G. Rusciano, A.C. De Luca, A. D'Alessio, P. Minutolo, G. Pesce, A. Sasso, *Carbon* 46 (2008) 335.
- [84] M. Alfè, B. Apicella, R. Barbella, J.-N. Rouzaud, A. Tregrossi, A. Ciajolo, *Proc. Combust. Inst.* 32 (2009) 697–704.
- [85] L.A. Sgro, G. Basile, A.C. Barone, et al., *Chemosphere* 51/10 (2003) 1079.
- [86] L.A. Sgro, A. Borghese, L. Speranza, et al., *Environ. Sci. Technol.* 42 (3) (2008) 859.
- [87] Cecere, L.A. Sgro, G. Basile, A. D'Alessio, A. D'Anna, P. Minutolo, *Combust. Sci. Technol.* 174 (11–12) (2002) 377.
- [88] R.A. Dobbins, C.M. Megaridis, *Langmuir* 3 (1987) 254.
- [89] R.A. Dobbins, H. Subramaniasivam, in: H. Bockhorn (Ed.), *Soot Formation in Combustion*, Springer-Verlag, Heidelberg, 1994, p. 290.
- [90] D'Alessio, A.C. Barone, R. Cau, A. D'Anna, P. Minutolo, *Proc. Comb. Inst.* 30 (2005) 2595.
- [91] R.A. Dobbins, R.A. Fletcher, H.-C. Chang, *Combust. Flame* 115 (1998) 285.
- [92] R.L. Vander Wal, *Combust. Flame* 112 (1998) 607.
- [93] R.L. Vander Wal, *Combust. Sci. Technol.* 118 (1996) 343.
- [94] A.C. Barone, A. D'Alessio, A. D'Anna, *Combust. Flame* 132 (2003) 181.
- [95] J. Israelachvili, *Intermolecular and Surface Forces*, Academic Press, London (UK), 1991.
- [96] W.H. Dalzell, A.F. Sarofim, *J. Heat Transfer* 91 (1969) 100.
- [97] H. Chang, T.T. Charalampopoulos, *Proc. Roy. Soc. London A* 430 (1990) 577.
- [98] A. De Filippo, L.A. Sgro, G. Lanzuolo, P. Minutolo, A. D'Anna, A. D'Alessio, Formation and growth of nanoparticles in non-sooting rich premixed flames, *Spring Meeting of the Western States Section of the Combustion Institute*, March 17 & 18, 2008, University of Southern California, USA, paper 08S-43.
- [99] L.A. Sgro, A.C. Barone, M. Commodo, A. D'Alessio, A. De Filippo, G. Lanzuolo, *Proc. Combust. Inst.* 32 (2009) 689–696.
- [100] A. D'Anna, M. Sirignano, M. Commodo, R. Pagliara, P. Minutolo, *Combust. Sci. Technol.* 180 (5) (2008) 950.
- [101] C.A. Echavarria, A.F. Sarofim, J. Lighty, A. D'Anna, *Proc. Combust. Inst.* 32 (2009) 705–711.
- [102] A. Tregrossi, A. Ciajolo, R. Barbella, *Combust. Flame* 117 (3) (1999) 553.
- [103] M. Alfè, B. Apicella, R. Barella, A. Tregrossi, A. Ciajolo, *Proc. Combust. Inst.* 31 (1) (2007) 585.
- [104] R.J. Santoro, H.G. Semerjian, R.A. Dobbins, *Combust. Flame* 51 (1983) 203.

- [105] R.J. Santoro, H.G. Semerjian, *Proc. Combust. Inst.* 20 (1984) 997.
- [106] J. Kent, H.G. Wagner, *Combust. Sci. Technol.* 41 (1984) 245.
- [107] R.J. Santoro, T.T. Yeh, J.J. Horvath, H.G. Semerjian, *Combust. Sci. Technol.* 53 (1987) 89.
- [108] K.C. Smyth, J.H. Miller, R.C. Dorfman, W.G. Mallard, R.J. Santoro, *Combust. Flame* 62 (1985) 157.
- [109] D.R. Honnery, J. Kent, *Combust. Flame* 82 (1990) 426.
- [110] M. Commodo, Diagnostic for the characterization of nanometric structures in high temperature reactive systems, *Ph.D. Thesis, University of Napoli "Federico II"*, December 2007.
- [111] J.Y. Hwang, S.H. Chung, *Combust. Flame* 125 (2001) 752.
- [112] N. Olten, S. Senkan, *Combust. Flame* 118 (3) (1999) 500.
- [113] D.B. Kittelson, *J. Aerosol Sci.* 29 (1998) 575.
- [114] M. Maricq, *J. Aerosol Sci.* 38 (1997) 1079.
- [115] S. Di Iorio, S.S. Merola, B.M. Vaglieco, A. D'Anna, E. Bichi, P. Minutolo, Emissions of ultrafine particles from a port fuel injection spark ignition engine *10th International Congress on Combustion By-Products and Their Health Effects*, Ischia, 17–20 June, 2007.
- [116] R. Barbella, C. Bertoli, A. Ciajolo, A. D'Anna, S. Masi, *SAE Trans. J. Engines* 3 (1989) 712.
- [117] A. Ciajolo, A. D'Anna, R. Barbella, C. Bertoli, M.V. Prati, In-cylinder study of soot and polycyclic aromatic hydrocarbon formation during the combustion cycle of a D.I. diesel engine burning tetradecane, *International Symposium COMODIA 90:639-644*, Kyoto, Japan, 1990.
- [118] R. Barbella, C. Bertoli, A. Ciajolo, A. D'Anna, *Proc. Combust. Inst.* 23 (1990) 1079.
- [119] B.M. Vaglieco, S.S. Merola, A. D'Anna, A. D'Alessio, *J. Quant. Spectr. Rad. Transfer* 73 (2–5) (2002) 443.
- [120] S. Kubo, *International Workshop on Combustion Generated Fine Carbon Particles*, Villa Orlandi, Italy, May 13–16, 2007.
- [121] P. Minutolo, A. D'Anna, M. Commodo, R. Pagliara, G. Toniato, C. Accordini, *Environ Eng. Sci.* 25 (10) (2008).
- [122] G. Toniato, C. Accordini, A. D'Anna, M. Commodo, P. Minutolo, R. Pagliara, Combustion characteristics of commercial burner for home appliance *Proceedings of Third European Combustion Meeting ECM 2007*, April 11–13, 2007, Crete (Greece).
- [123] I.M. Kennedy, *Prog. Energy Combust. Sci.* 23 (1997) 95.
- [124] M. Frenklach, H. Wang, *Proc. Combust. Inst.* 23 (1990) 1559.
- [125] M. Frenklach, *Phys. Chem. Chem. Phys.* 4 (2002) 2028.
- [126] A. D'Anna, A. Violi, A. D'Alessio, A.F. Sarofim, *Combust. Flame* 127 (1/2) (2001) 1995.
- [127] H. Richter, S. Granata, W.H. Green, J.B. Howard, *Proc. Combust. Inst.* 30 (2005) 1397.
- [128] A. D'Anna, J. Kent, *Combust. Flame* 152 (2008) 573.
- [129] A. D'Anna, *Energy Fuels* 22 (3) (2008) 1610.
- [130] J. Singh, R.I.A. Patterson, M. Kraft, H. Wang, *Comb. Flame* 145 (1–2) (2006) 117.
- [131] M.D. Smooke, C.S. McEnally, L.D. Pfefferle, R.J. Hall, M.B. Colket, *Comb. Flame* 117 (1–2) (1999) 117.
- [132] J. Appel, H. Bockhorn, M. Frenklach, *Combust. Flame* 121 (2000) 122.
- [133] J. Kent, Prediction of particulates in turbulent diffusion flames by conditional moment closure, *International Workshop on Combustion Generated Fine Carbon Particles*, Villa Orlandi, Italy, May 13–16, 2007.
- [134] M. Frenklach, D.W. Clary, W.C. Gardiner Jr., S.E. Stein, *Proc. Combust. Inst.* 20 (1985) 887.
- [135] M. Frenklach, H. Wang, in: H. Bockhorn (Ed.), *Soot Formation in Combustion: Mechanisms and Models*, Springer-Verlag, Heidelberg, 1994, p. 165.
- [136] M. Frenklach, *Chem. Eng. Sci.* 40 (1985) 1843.
- [137] A. Kazakov, M. Frenklach, *Combust. Flame* 114 (1998) 484.
- [138] M. Frenklach, S.J. Harris, *J. Colloid Interface Sci.* 118 (1987) 252.
- [139] M.B. Colket, R.J. Hall, in: H. Bockhorn (Ed.), *Soot Formation in Combustion: Mechanisms and Models*, Springer-Verlag, Heidelberg, 1994, p. 442.
- [140] C.J. Pope, J.B. Howard, *Aerosol Sci. Technol.* 27 (1997) 73.
- [141] G. Blanquart, H. Pitsch, A jointvolume-surface-hydrogen multi-variate model for soot formation, *International Workshop on Combustion Generated Fine Carbon Particles*, Villa Orlandi, Italy, May 13–16, 2007.
- [142] F. Mauss, K. Netzell, C. Marchal, G. Moréac, Particle size distribution functions in laminar and turbulent flames, *International Workshop on Combustion Generated Fine Carbon Particles*, Villa Orlandi, Italy, May 13–16, 2007.
- [143] D.A. McQuarrie, J.D. Simon, *Physical Chemistry A Molecular Approach*, University Science Books, Sausalito, California, USA, 1997.
- [144] V.M.H. Lavanchy, H.W. Gaggeler, U. Schotterer, M. Schwikowski, U. Baltensperger, *J. Geophys. Res.* 104 (21) (1999) 227.